Model Predictive Control—A Simple and Powerful Method to Control Power Converters

Samir Kouro, *Member, IEEE*, Patricio Cortés, *Member, IEEE*, René Vargas, *Student Member, IEEE*, Ulrich Ammann, *Member, IEEE*, and José Rodríguez, *Senior Member, IEEE*

***Abstract*—This paper presents a detailed description of Finite Control Set Model Predictive Control (FCS-MPC) applied to power converters. Several key aspects related to this methodology are, in depth, presented and compared with traditional power converter control techniques, such as linear controllers with pulsewidth-modulation-based methods. The basic concepts, operating principles, control diagrams, and results are used to provide a comparison between the different control strategies. The analysis is performed on a traditional three-phase voltage source inverter, used as a simple and comprehensive reference frame. However, additional topologies and power systems are addressed to highlight differences, potentialities, and challenges of FCS-MPC. Among the conclusions are the feasibility and great potential of FCS-MPC due to present-day signal-processing capabilities, particularly for power systems with a reduced number of switching states and more complex operating principles, such as matrix converters. In addition, the possibility to address different or additional control objectives easily in a single cost function enables a simple, flexible, and improved performance controller for power-conversion systems.**

***Index Terms*—Adjustable-speed drives, current control, model predictive control (MPC), power converters, pulsewidth modulation (PWM).**

I. Introduction

POWER converters and drive control technology have been in continuous development since the second half of the 20th century and have proven to be enabling technologies in practically every application area (energy, communications, medicine, mining, transportation, etc.). In particular, converter control techniques have been a very active research topic in the field of power electronics, covering countless topologies for low-, medium-, and high-power applications [1]–[4]. Classic linear controllers, together with modulation schemes and nonlinear controllers based on hysteresis comparators, have been the most widely analyzed and developed control strategies for power converters [2]. This can be explained by the limitation imposed initially by the analog implementation of control loops. These control methods were later on adapted to discrete time digital implementations, which are currently widely accepted as the industry standard.

On the other hand, digital signal processing has experienced an even more explosive evolution over the last decades, enabling the implementation of emerging and, usually, more complex control techniques. Some of these methods have been applied to power converters, among them fuzzy [5], [6], adaptive [7], [8], sliding-mode [9], [10], and predictive controls. The latter is a wide control concept that can be further subdivided or classified into several categories [11], depending on the operating principle and other characteristics. In general terms, predictive control can be considered as any algorithm that uses a model of the system to predict its future behavior and selects the most appropriate control action based on an optimality criterion. One of the earlier predictive controllers used in power converters is the so-called dead-beat control, which eliminates the classic linear controller by using a predictive model of the system. This model is used to calculate the required reference voltage in order to reach the desired reference value for a certain variable (usually the current). The predicted reference voltage is later generated by the converter via a modulation stage. This scheme has been applied for current control of inverters [12]–[19], rectifiers [20], [21], active filters [22], [23], and uninterruptible power supplies (UPSs) [24], [25].

A different approach is Model Predictive Control (MPC) [26], in which a model of the system is considered in order to predict the future behavior of the variables over a time frame (integer multiple of the sample time). These predictions are evaluated based on a cost function, and then, the sequence that minimizes the cost function is chosen, obtaining, in this way, the future control actions. Only the first value of the sequence is applied, and the algorithm is calculated again every sampling period. MPC has several advantages, such as the easy inclusion of nonlinearities and constraints. This scheme has few applications in power converter control and drives due to the high amount of calculations needed in order to solve the optimization problem online, which is incompatible with the small sampling times used in converter control. One solution in order to reduce the calculation time is to solve the optimization problem offline, as presented in [27], where MPC is implemented as a search tree and the calculation time is reduced, making it possible to use the MPC in drive control. Another solution is the use of Generalized Predictive Control (GPC) [28], where the optimization is solved analytically, obtaining a linear controller. Nevertheless, with GPC, it is very difficult to include system constraints and nonlinearities.

Manuscript received May 9, 2008; revised September 30, 2008. First published November 18, 2008; current version published June 3, 2009. This work was supported in part by the Universidad Técnica Federico Santa María, in part by Ryerson University, and in part by the Chilean National Fund of Scientific and Technological Development (FONDECYT) under Grant 1080582.

S. Kouro was with the Electronics Engineering Department, Universidad Técnica Federico Santa María, 2390123 Valparaíso, Chile. He is now with the Department of Electrical and Computer Engineering, Ryerson University, Toronto, ON M5B 2K3, Canada (e-mail: samir.kouro@ieee.org).

P. Cortés, R. Vargas, and J. Rodríguez are with the Electronics Engineering Department, Universidad Técnica Federico Santa María, 2390123 Valparaíso, Chile (e-mail: patricio.cortes@usm; rene.vargas@usm.cl; jrp@usm.cl).

U. Ammann is with the Institute of Power Electronics and Control Engineering, Universität Stuttgart, 70569 Stuttgart, Germany (e-mail: ammann@ilea.uni-stuttgart.de).

Digital Object Identifier 10.1109/TIE.2008.2008349

Another approach for implementing MPC for power converters and drives is to take advantage of the inherent discrete nature of power converters. Since power converters have a finite number of switching states, the MPC optimization problem can be simplified and reduced to the prediction of the system behavior only for those possible switching states. Then, each prediction is used to evaluate a cost function (also known as quality or decision function), and consequently, the state with minimum cost is selected and generated. This approach is known as a Finite Control Set MPC (FCS-MPC), since the possible control actions (switching states) are finite. This method is also known as finite alphabet MPC or simply as predictive control, and it has been successfully applied to a wide range of power converter and drive applications [29]–[56].

In this paper, a general approach on FCS-MPC of power converters and drives is presented. This paper has, in part, a survey nature, addressing the latest advances and promising future of this technology. In addition, a comparison between FCS-MPC and classic linear controllers is presented. Special attention is given to conceptual differences in the operating principle, controller design, and implementation. The traditional two-level voltage-source inverter (2L-VSI) has been selected as the main topology for comparison. The reasons are its more generic structure, simple operating principle, and industrial presence. In addition, this topology is somehow neutral to both control techniques, which means that it has no special features or favorable characteristics that will make one method outperform another, providing a fair reference frame for the analysis. In addition, other converter topologies, drives, and applications are addressed to show the flexibility and potentiality of FCS-MPC.

II. FCS-MPC Operating Principle

The power converter or drive control problem can be defined as the determination of an appropriate control action $S(t)$ (usually the gate signals of the converter) that will drive a generic system variable $x(t)$ as close as possible to a desired reference value $x^*(t)$. Consider the qualitative behavior of $x(t)$ and its regularly sampled value $x(t_k)$ over a sample period T_s for a system with a finite number of control actions n, as shown in Fig. 1(a), where measurements, computations, and control actions are performed instantly (ideal case). Since the control actions or control set is finite in number S_i, with $i = 1, \ldots, n$, they can be evaluated together with the measured value $x(t_k)$, based on a prediction function f_p, to predict all the possible system transitions $x_{pi}(t_{k+1}) = f_p\{x(t_k), S_i\}$, for $i = 1, \ldots, n$. This prediction function is directly derived from the discrete model and parameters of the system. To determine which of the control actions is to be selected, a decision or cost function f_g can be defined, usually dependent on the desired reference value and the predictions $g_i = f_g\{x^*(t_{k+1}), x_{pi}(t_{k+1})\}$, for $i = 1, \ldots, n$. Note that the future reference value is needed $x^*(t_{k+1})$, which can be assumed to be equal to the actual value $x^*(t_k)$, since T_s is sufficiently small compared with the dynamic behavior of the system, and thus, the reference can be considered constant over T_s. If needed for highly dynamic systems, the future reference value $x^*(t_{k+1})$ can be estimated via appropriate extrapolation methods. A typical example for

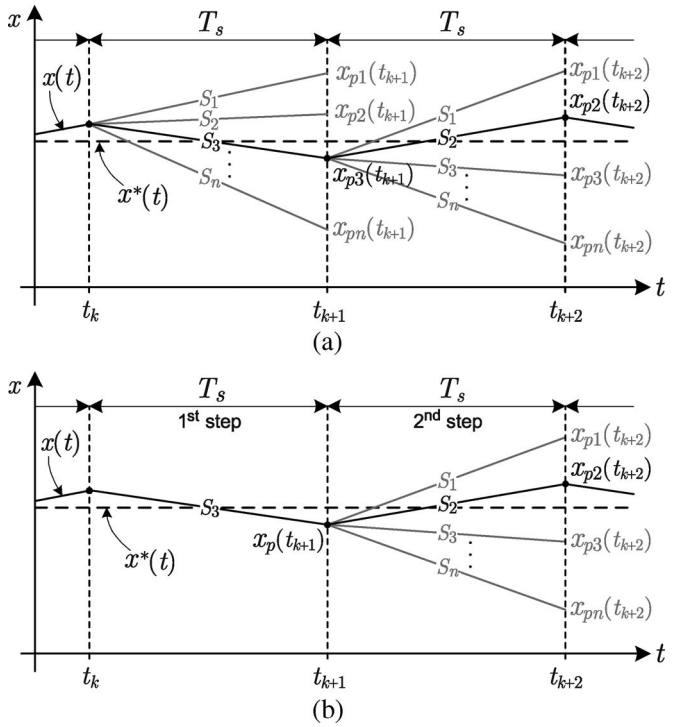

Fig. 1. FCS-MPC operating principle. (a) Ideal theoretical case. (b) Implementation case.

f_g would be the absolute error between the predictions and the reference $g_i = |x^*(t_{k+1}) - x_{pi}(t_{k+1})|$. The evaluation of the cost function with the n predictions will lead to n different costs. Naturally, the control action leading to the minimum cost ($\min\{g_i\}$, for $i = 1, \ldots, n$) is selected to control the system.

Based on the example shown in Fig. 1(a), the predicted value $x_{p3}(t_{k+1})$ is the closest to the reference $x^*(t_{k+1})$; hence, S_3 is selected and applied in $t = t_k$. Following the same criterion, S_2 is selected and applied in $t = t_{k+1}$. However, the ideal theoretical case in which the variables can be measured, predicted, and controlled instantly in $t = t_k$ is not realizable in real-time applications. Nevertheless, this problem can be overcome if a two-step-ahead prediction is considered, as shown in Fig. 1(b), in which the control action to be applied in the following sample time $S(t_{k+1})$ is determined. This way, a complete sample period T_s is available to perform the algorithm. Naturally, the sample period T_s has to be greater than the measurement, computation, and actuation times added together.

Assume that on a sample time t_k, a measurement $x(t_k)$ is made and the previously computed control action $S(t_k)$ is applied. With this information and the system model, a first prediction can be made to obtain the future value $x(t_{k+1})$ (this is the first step prediction). Now, from the predicted value $x_p(t_{k+1})$, the FCS-MPC algorithm is performed for n possible control actions, leading to one optimal selection $S(t_{k+1})$ (this is the second step prediction). Both predictions are performed during the first sample period, and then, at $t = t_{k+1}$, the optimal selected control action $S(t_{k+1})$ is applied, while $x(t_{k+1})$ is measured to perform the algorithm again. As shown in the example in Fig. 1(b), there is only one prediction for the first step, given by the applied control action $S(t_k) = S_3$ determined in the previous execution of the algorithm,

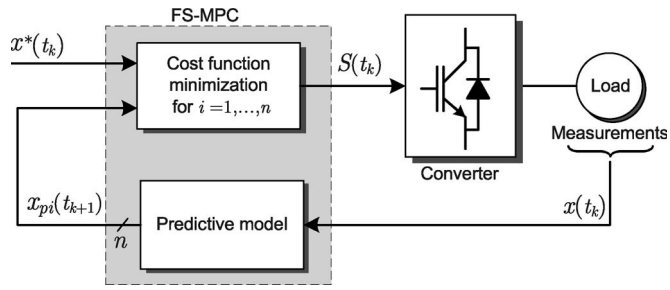

Fig. 2. FCS-MPC generic control diagram.

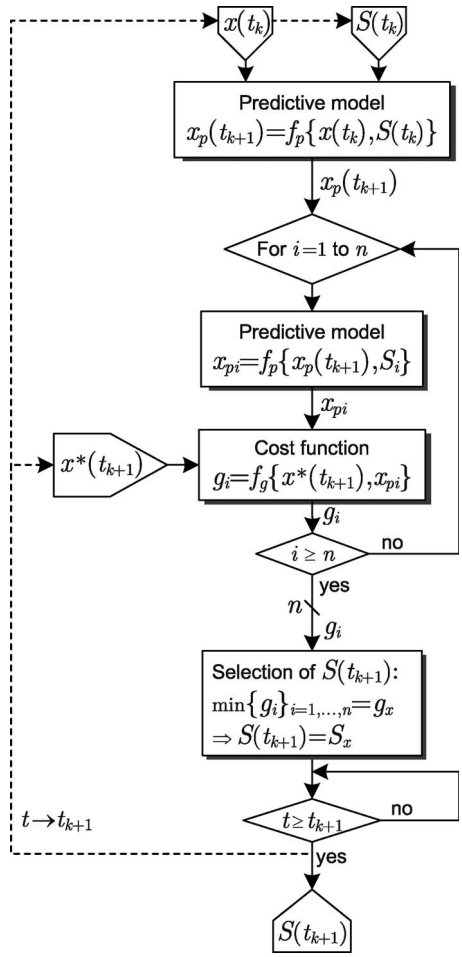

Fig. 3. FCS-MPC generic algorithm.

while $S(t_{k+1}) = S_2$ is selected from the n predictions for the second step.

A simplified control block diagram and the corresponding algorithm for the real-time implementation of FCS-MPC are shown in Figs. 2 and 3, respectively, considering a generic system variable $x(t)$. It is worth mentioning that this control method is not limited to a single variable; on the contrary, multiple variables, system constraints, perturbations, saturations, and, basically, every characteristic that can be mathematically modeled and measured can be included in the predictive model and cost function. This is the basis of the great flexibility and control potential that can be achieved with FCS-MPC. Moreover, the fact that power converters have a reduced and limited number of switching states (or control set) makes this

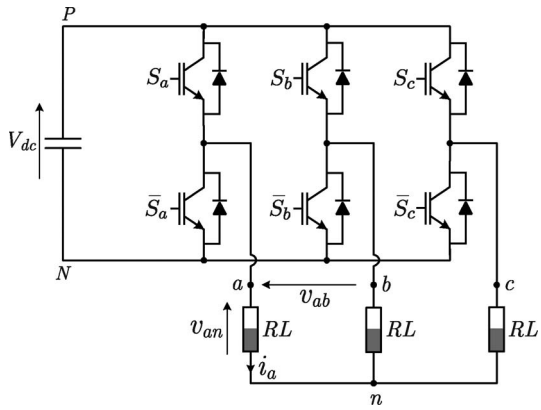

Fig. 4. VSI power circuit.

method feasible to implement with present-day available microprocessing resources. Since only a discrete model of the system is necessary, rather than approximated linear models together with control system design theory and modulation algorithms, a simpler and more direct design and implementation of the controller can be achieved.

III. Comparison of Classic Linear PI and FCS-MPC

To highlight the conceptual differences of the FCS-MPC approach with traditional control methods, a comparison of the current control of a 2L-VSI is presented in this section. The 2L-VSI has been selected since it is one of the most widespread converter topologies in the industry and features a generic structure and operating principle that can be easily extended to other converter topologies.

A. Power Converter Overview

The power circuit of a 2L-VSI is shown in Fig. 4. For simplicity, a passive-diode front-end rectifier is assumed to provide the dc-link voltage $V_{\rm dc}$. The converter consists of three phase legs, which can connect the corresponding load terminals to the positive (P) or negative (N) bars of the converter by controlling the two power switches of a leg with $S_x = 1$ and $S_x = 0$ $(x = a, b, c)$. Since there are three phases and each phase features two control actions, there are $2^3 = 8$ different switching states. If a voltage space vector is defined as

$$\mathbf{v}_s = \frac{2}{3} V_{\rm dc}(S_a + aS_b + a^2 S_c) \tag{1}$$

where $a = e^{j2\pi/3}$; then, evaluating the different switching states, eight voltage space vectors can be generated by the converter $(\mathbf{v}_0, \ldots, \mathbf{v}_7)$, as shown in Fig. 5. For this comparison, a linear resistive inductive RL load is considered.

B. Linear PI Current Control With Space Vector Modulation (SVM) of a 2L-VSI

The traditional current control for a VSI is composed of two stages, a linear proportional–integral (PI) controller followed by a modulation stage, usually pulsewidth modulation (PWM) or SVM [2]. For the PI controller design, the converter is

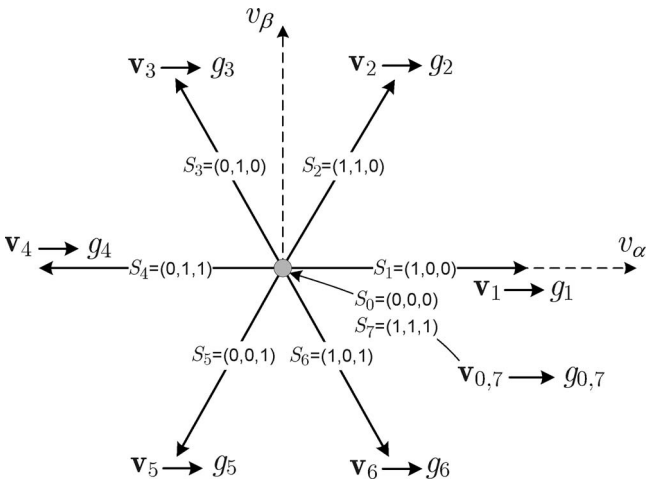

Fig. 5. VSI voltage space vectors, switching states, and cost function dependence.

neglected, and a transfer function is obtained from the RL load model

$$\mathbf{v}_s = R\mathbf{i}_s + L\frac{d\mathbf{i}_s}{dt} \quad \xrightarrow{\mathcal{L}} \quad G(s) = \frac{\mathbf{i}_s}{\mathbf{v}_s} = \frac{1}{Ls+R} \tag{2}$$

where $\mathcal{L}$ is the Laplace transform. The PI controller transfer function is

$$C(s) = K_p\left(1 + \frac{1}{T_i s}\right) \tag{3}$$

where K_p and T_i are the proportional and integral parameters, respectively, which can be designed via pole placement or root locus procedures [57]. Two PI controllers are necessary, one for the i_α and one for the i_β component of $\mathbf{i}_s$ or i_d and i_q components if a rotating frame for $\mathbf{i}_s$ is considered (depending on the application). The output of the controller is the voltage vector that is necessary to correct the current trajectory. This reference voltage vector $\mathbf{v}_s^*$ is then modulated by the converter with PWM or SVM [2]. Particularly discontinuous SVM has become the standard method for the modulation stage [58]. A simplified control diagram of this method is shown in Table I.

Note that for the chosen example, the load is linear; hence, its model and the corresponding control has no further complications. However, the converter has saturation (maximum voltage and current) which is a nonlinear condition generally overcome with antiwindup algorithms. Other converters, loads, and, in particular, motor drives, are highly nonlinear systems which complicate the obtention of an approximated linearized transfer function for the controller design, leading to robustness issues. In addition, the implementation of the PI controller in the present-day digital platforms demands discretization of the controller. Moreover, neglecting the converter assumption held during the design process is valid only if a high-bandwidth modulation stage is implemented, which is true for high switching frequencies, hence introducing higher losses and demanding more digital processing power. A favorable characteristic is the fact that the PWM- or SVM-based modulation stage imposes a fixed average switching frequency.

C. Current FCS-MPC of a 2L-VSI

The FCS-MPC current control problem can be easily derived from the generic operating principle analyzed in Section II. The variable $x(t)$ would be the current $\mathbf{i}_s$; the control action $S(t)$ represents the switching states (S_i, with $i = 0, \ldots, 7$) of the converter shown in Fig. 5. The predictive model corresponds to the discrete time model of the load, with a Euler approximation of the current derivative, which leads to

$$\mathbf{i}_{\text{sp}}\{S_i\} = \frac{L\mathbf{i}_s(t_k) + T_s\mathbf{v}_i(t_{k+1})}{RT_s + L} \tag{4}$$

$$\mathbf{v}_i(t_{k+1}) = \frac{2}{3}V_{\text{dc}}\left(S_i \cdot [1 \quad a \quad a^2]^{\text{T}}\right) \tag{5}$$

where $\mathbf{i}_s(t_k)$ is the measured current and $\mathbf{v}_i(t_{k+1})$ is the voltage vector generated by the switching states S_i, with $i = 0, \ldots, 7$. In addition, note that $\mathbf{i}_{ps} = i_{\alpha p} + ji_{\beta p}$. Finally, the cost function that needs to be minimized is

$$g_i(t_k) = \left|i_\alpha^* - i_{\alpha p}\{S_i\}\right| + \left|i_\beta^* - i_{\beta p}\{S_i\}\right|. \tag{6}$$

The corresponding simplified block diagram of the current FCS-MPC is shown in Table I.

To further show how the algorithm works, Fig. 6(a) and (b) shows the system behavior in time and space vector representations, respectively. The shadowed region corresponds to a two-step current prediction, such as the one shown previously in Fig. 1(b). Note that, now, two variables are controlled with one cost function (6). From the space vector waveforms, it can be clearly appreciated that some pairs of vectors produce the same effect on the α component; $\mathbf{v}_2$ and $\mathbf{v}_6$, for example, produce an increase of i_α, while $\mathbf{v}_3$ and $\mathbf{v}_5$ produce a reduction. In addition, $\mathbf{v}_1$ and $\mathbf{v}_4$ produce a higher increase and higher reduction, respectively. For example, this explains why in the time representation, $i_{\alpha p}\{\mathbf{v}_1\}$ is above all the other current predictions. As expected, the zero vectors $\mathbf{v}_0$ and $\mathbf{v}_7$ do not change i_α at all. In a similar way, i_β is increased by $\mathbf{v}_2$ and $\mathbf{v}_3$, reduced by $\mathbf{v}_5$ and $\mathbf{v}_6$, and kept equal by $\mathbf{v}_0$, $\mathbf{v}_1$, $\mathbf{v}_4$, and $\mathbf{v}_7$.

Based on the predictions shown in Fig. 6(a), for i_α, the selected vectors are $\mathbf{v}_2$ and $\mathbf{v}_6$, while for i_β, the chosen vectors are $\mathbf{v}_2$ and $\mathbf{v}_3$; hence, the overall selection to fulfill both conditions is $\mathbf{v}_2$, which can be clearly appreciated as the optimal choice in Fig. 6(b).

Although it cannot directly be observed in this illustrative example, FCS-MPC does not force a commutation in each sample period. Hence, the average switching frequency is variable, leading to a spread current spectrum. Nevertheless, this drawback can be easily compensated, as will be discussed later.

A summary of the most distinctive characteristics of both analyzed methods is given in Table I. Simulation results of the dynamic behavior of the load current shown in the table are obtained in both cases under the same operating conditions. These results were obtained using Matlab/Simulink, with a sample period of $T_s = 100\ \mu$s. A step change at $t = 0.035$ s is performed only on the α component of the current from 13 to 2.6 A. Both methods seem to behave comparably under this situation. However, the step in the α component produces a coupling effect in the β component for the PI with the SVM control algorithm, while in FCS-MPC, this effect does not appear.

TABLE I
COMPARISON BETWEEN CLASSICAL LINEAR CONTROLLERS (INCLUDING MODULATION) AND FCS-MPC

Item description	Linear controller + Modulation	FCS-MPC
Control diagram	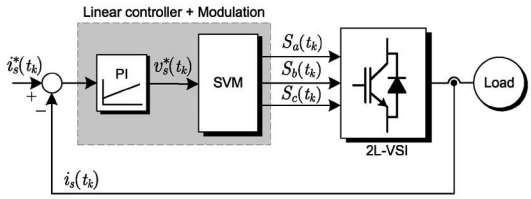	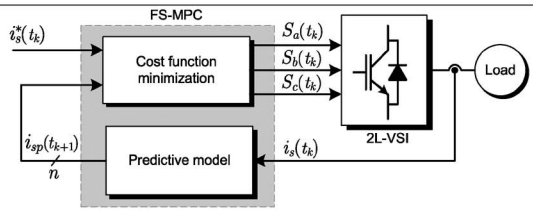
Model	Linear load model (for PI design), inverter model (for SVM)	Discrete time load-inverter model (for prediction)
Controller design	PI parameter adjustment (root locus or pole placement)	Cost function definition
Modulation	PWM or SVM	no modulation
Implementation	Analogical or digital (after controller discretization)	Direct digital implementation
Switching freq.	Fixed	Controllable (variable or fixed)
Multivariable	Coupled	Decoupled
Flexibility	Constraint inclusion is not straight forward	Constraints can be included directly in the cost function
Sim. results: step in i_α	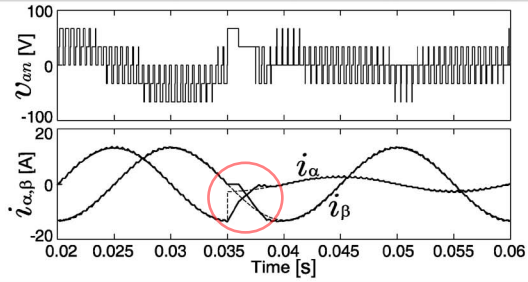	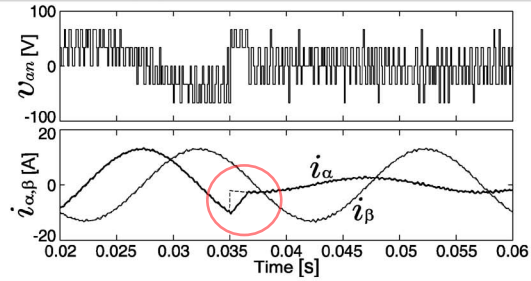

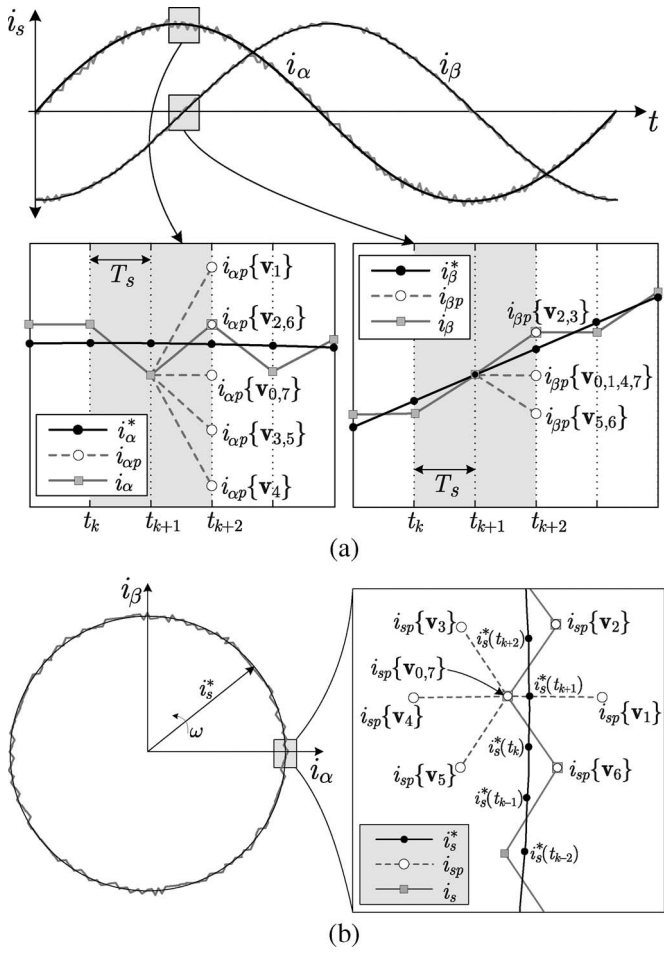

Fig. 6. FCS-MPC current control operating principle. (a) Time representation of i_α and i_β control. (b) Space vector representation of $i_s = i_\alpha + ji_\beta$ control.

An in-depth comparison and assessment on this topic is presented in [59].

IV. COST FUNCTION FLEXIBILITY AND POTENTIAL

Traditional linear controllers with modulation are limited due to their classic feedback structure. Moreover, the bandwidth and robustness of the controller will depend on how dominant the nonlinearities of the system are. FCS-MPC, on the other hand, uses a full prediction model of the system, and the feedback is included in the cost function, which is not limited to the magnitude of the error of the controlled variable, as analyzed in the example of Section III. In fact, the errors can be measured with functions such as

$$g = |x^* - x_p| \tag{7}$$

$$g = [x^* - x_p]^2 \tag{8}$$

$$g = \frac{1}{T_s}\int_0^{T_S} [x^*(t) - x_p(t)]\, dt. \tag{9}$$

The difference between (7) and (8) is that the latter produces an overproportional cost (in powers of two), producing a higher penalization of bigger errors compared with smaller ones. This can be used to control variables closer to the reference and reduce ripple amplitude. In essence, this error measure will produce a faster controller for the specific variable in the cost function; however, it will also introduce higher switching frequencies. Cost function (9) takes into account the whole prediction during T_s, not only the final value at t_{k+1}; hence, the mean value of the variable is closer to the reference, resulting in more accurate reference tracking. Considering fast sample

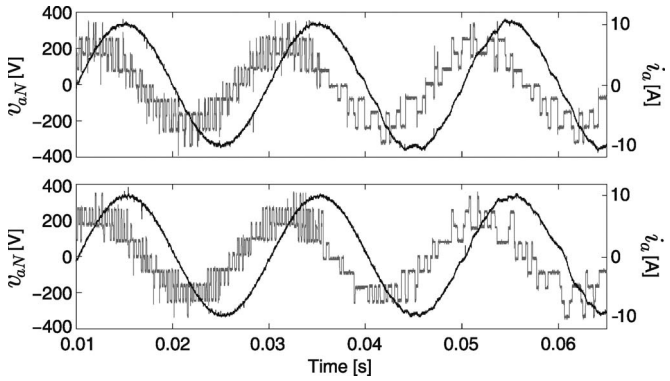

Fig. 7. Experimental current control of an NPC converter (power circuit in Fig. 13) with switching frequency reduction at $t = 0.035$ s. (Top) PI with PWM and (bottom) FCS-MPC.

periods, as is usual in power converters and drives control, the three cost measures do not have noticeable differences in their performances. Hence, for simplicity and computational effort reduction, (7) will fit most of the applications.

A. Switching Frequency and Efficiency

An important issue in power conversion, particularly in high-power applications, is the efficiency of the power converter, due to the amount of power loss in long-term operations and cooling system costs. Switching losses are particularly relevant, since they are produced by the commutation of the power devices; hence, they are a direct result of the control of a modulation method. In FCS-MPC, switching losses can be controlled by adding another term to the cost function g. Three approaches have been analyzed, namely, the reduction of commutations by predicting the number of switchings involved in using each switching state, the prediction of the switching losses caused by selecting each switching state, and the assurance of a number of commutations in a certain period of time to obtain an imposed switching frequency. These alternatives are reflected, respectively, in the following three additional terms in the quality functions:

$$g' = g + \lambda \cdot C_p \tag{10}$$

$$g' = g + \lambda \cdot \sum_{j=1}^{n} \Delta i_{cp}(j) \cdot \Delta v_{cep}(j) \tag{11}$$

$$g' = g + \lambda \cdot \left| \bar{f}^*_{\mathrm{sw}} - \frac{1}{\Delta t} \sum_{i=0}^{\frac{\Delta t}{T_s}-1} C(t_{k-i}) \right| \tag{12}$$

where λ is a weighting factor. In (10), C_p is the number of the semiconductors' commutations involved when changing from the present to the future switching state [50]. This new component in the cost function will avoid those switching states that would produce more commutations. Fig. 7 shows an experimental comparison between the classic controller (including PWM-based modulation) and the FCS-MPC for a current control of a neutral-point-clamped (NPC) multilevel converter. This result has been obtained with a Dspace DS1104 control board with Matlab/Simulink installed on a host standard personal computer. The sample period used to implement this strategy is $T_s = 100$ μs. At $t = 0.035$ s, a reduction is introduced in the carrier frequency of the PWM method, and the weight factor λ is set at a value different from zero, achieving, for both methods, a reduction in the average switching frequency. It can be clearly appreciated that both algorithms have very similar performances.

In the second case, cost function (11), the terms $\Delta i_{cp}(j)$ and $\Delta v_{cep}(j)$ are the predicted changes in the collector's current and the collector–emitter voltage of the semiconductor j, respectively, considering a converter with n semiconductors. Hence, the switching losses proportional to $\Delta i_c \cdot \Delta v_{ce}$ of each semiconductor are considered directly in the cost function. Consequently, switching-state transitions that imply fewer switching losses will be then preferred [56]. The third alternative (12) imposes an average switching frequency given as a reference $\bar{f}^*_{\mathrm{sw}} = C^*/\Delta t$, where C^* is the number of desired commutations during Δt, an arbitrary time frame multiple of the sample period T_s. The reference $\bar{f}^*_{\mathrm{sw}}$ is subtracted with the sum of the previous number of commutations performed during Δt (including the present prediction of the switching-state transitions under evaluation in the cost function). This quality function will select those switching states that maintain the average switching frequency as close as possible to the desired value, controlling the converter's switching frequency.

B. Common-Mode Voltage

Common-mode voltages produced by power converters feeding electric machines cause overvoltage stress to the winding insulation, affecting its lifetime and producing deterioration. A strategy to reduce and control common-mode voltages from switched-mode power converters using FCS-MPC has been introduced in [55]. The working principle is to add an additional term with the prediction of the common-mode voltage v_{cmp} to the quality function g, resulting in

$$g' = g + \lambda \cdot |v_{cmp}|. \tag{13}$$

This way, the method will associate a cost to switching states that produce more common-mode voltages. The prediction of the common-mode voltage v_{cmp} is obtained by using the output voltages per phase, which each switching state under evaluation would produce

$$v_{cmp} = \frac{v_{aNp} + v_{bNp} + v_{cNp}}{3}. \tag{14}$$

Experimental results showing the FCS-MPC mitigation of the common-mode voltages in a matrix converter is shown in Fig. 8. This result has been obtained with a Dspace DS1103 control board with Matlab/Simulink installed on a host standard personal computer. The sample period used to implement this strategy is $T_s = 8$ μs. The corresponding weighting factor λ is set at a different value from zero at $t = 0.03$ s, to highlight the behavior before and after the compensation.

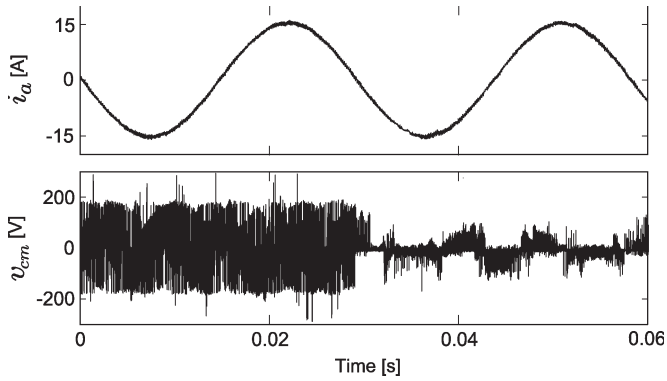

Fig. 8. Experimental current control of a matrix converter (power circuit in Fig. 17) using FCS-MPC, with the common-mode voltage compensation activated at $t = 0.03$ s. (Top) Load current. (Bottom) Common-mode voltage.

C. FCS-MPC With Spectrum Shaping

Since regular FCS-MPC chooses the optimal switching state that minimizes a cost function, no commutations are forced every sample period. In fact, one switching state can be the optimal selection for two or more sample periods. This leads to a variable switching frequency, which can cause resonances, vibrations, and acoustic noise, depending on the application.

This drawback can be overcome in FCS-MPC by simply introducing frequency information into the cost function. For example, consider a general variable $x(t)$, with the frequency weighted cost function

$$g = F_z\{x^* - x_p\} \tag{15}$$

where F_z is a discrete time filter. It can be said that the filter somehow "hides" information in the cost function for those frequencies for which it is designed. Hence, the switching-state transitions producing harmonic components in those frequencies will be selected, since there is no or little cost associated to them. As a consequence, the filter can be designed in such a way that the desired harmonic content can be imposed in the system variables, enabling the spectrum shaping.

For power converters, it could be particularly interesting to produce fixed switching frequencies for which a narrowband stop filter (Notch) can be used [38]. Fig. 9(a) shows a filter designed to eliminate all the information around 4 kHz in the cost function. Using the approach of (15) in the current control cost function (6) for a 2L-VSI leads to the imposed current spectrum experimental results shown in Fig. 9(b). This result has been obtained with a TMS320F2812 DSP. The sample period used to implement this strategy is $T_s = 30\ \mu$s.

Instead of fixing the switching frequency, it can also be of interest to reduce the harmonic content for electromagnetic interference and electromagnetic compatibility purposes. In this case, other filter structures can be used in the cost function [40].

D. Reactive Input Power Control

With the FCS-MPC approach, the objective of controlling the reactive input power Q can be achieved by simply penalizing switching states that produce predictions of Q distant from the reference value Q^*. This method produces, as a consequence,

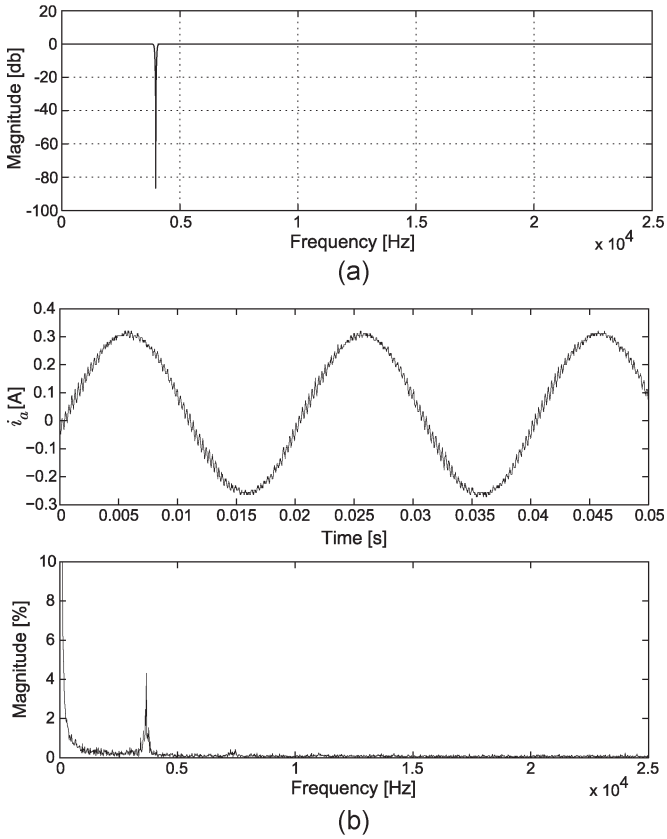

Fig. 9. Experimental FCS-MPC of a 2L-VSI with spectrum shaping. (a) Notch filter on 4 kHz. (b) Experimental results for load current and its spectrum.

the control of the input power factor. This can be simply achieved by including in the original quality function g an additional term

$$g' = g + \lambda \cdot |Q^* - Q_p| \tag{16}$$

where Q_p is the predicted reactive input power, calculated based on predictions of the input current and voltage by

$$Q_p = Im\{\mathbf{v}_{\rm sp} \cdot \bar{\mathbf{i}}_{\rm sp}\} = v_{\beta p} \cdot i_{\alpha p} - v_{\alpha p} \cdot i_{\beta p} \tag{17}$$

where $\mathbf{v}_{\rm sp}$ and $\mathbf{i}_{\rm sp}$ are the input voltage and current space vector predictions, respectively. Note that $\bar{\mathbf{i}}_{\rm sp}$ is the complex conjugate of vector $\mathbf{i}_{\rm sp}$. Since line voltages are low-frequency signals, the method can be simplified, considering the prediction to be equal to the last measured value of the variable, i.e., $\mathbf{v}_{\rm sp} \approx \mathbf{v}_s$. Generally, an operation with unity power factor is desired; hence, $Q^* = 0$. Thus, the additional term is reduced to $|Q_p|$. For further details, please refer to [29], [34]–[36], and [54].

V. FCS-MPC Challenges

As mentioned before, different variables can be included in a single cost function. They can be even of different physical natures (current, voltage, reactive power, switching losses, torque, flux, etc.). Since some variables have completely different values than others, mainly because they are expressed in different units (e.g., the maximum current error can be 1 A, while the voltage error can be 10 V), this can lead to coupling effects or

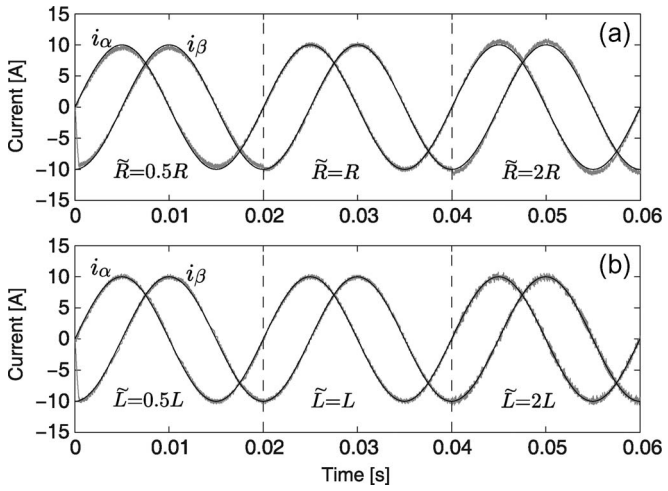

Fig. 10. FCS-MPC of a 2L-VSI under parameter variation or modeling error (simulation). (a) Error in the load resistance. (b) Error in the load inductance.

to changes in the relative importance of one variable over the other in the cost function. A simple way to address this issue is to include a coefficient or weight factor λ for each variable in the cost function

$$g = \lambda_x|x^* - x_p| + \lambda_y|y^* - y_p| + \cdots + \lambda_z|z^* - z_p|. \quad (18)$$

At the present state of the art, the coefficients of the cost function are determined by empirical procedure. There is no analytical or numerical solution proposed yet to obtain an optimal solution to the problem for FCS-MPC. In [63], some guidelines are presented to help the weighting factor design process. This challenge is an open research topic for future contributions to FCS-MPC.

In this paper, only two-step-ahead predictions have been presented. However, there is no theoretical limit to the number of predictions that can be performed. It is expected that with more predictions in advance, more knowledge of the system is considered in the cost function. However, practical implementations are limited by the computational requirements of the algorithm, which will impose a maximum number of realizable predictions. Moreover, it has been shown that the performance improvement from using one to two step predictions is important but is negligible when comparing two- with three- (or more) step-ahead predictions [26].

Like in all control theories, measurement noise and parameter uncertainty (or variability under operation) can degrade the control system performance and even affect system stability. This is also true for FCS-MPC. Although several publications have addressed this issue, showing appropriate system behavior in the presence of parameter variations and measurement noise [32], [61], there is still not enough comparable information to conclude whether FCS-MPC performs better or worse in this aspect than classical linear-modulation controllers. Fig. 10(a) and (b) shows the behavior of a current controller for a 2L-VSI with FCS-MPC under parameter variation or modeling error of the load resistance and inductance, respectively. These simulation results were obtained using Matlab/Simulink, with a sample period $T_s = 100\ \mu$s. Note that each waveform is divided into three parts; for example, in Fig. 10(a), the first part shows the current obtained when the model resistance $\tilde{R}$ is half of the real resistance R, the middle shows the model that is correct, and the last shows that the resistance of the prediction model is the double of the real one. The same was tested for the load inductance in Fig. 10(b). Note that in both cases, despite the huge modeling errors of 50% and 100%, respectively, the current is properly controlled with negligible differences. There seems to be an amplitude error in the case of the resistance model error while higher ripple is obtained for the case of the inductance model error.

A theoretical approach or analysis in relation to the robustness of FCS-MPC of power converters and drives has not been reported, to date, and is a possible field of research and development.

Another unexplored issue of FCS-MPC of power converters is the effective bandwidth achieved by the controller. Related theoretical analyses or frequency-response measurements have not been reported, to date. This is not trivial, considering the fact that FCS-MPC is inherently a nonlinear control algorithm, in the same sense as the hysteresis controllers; hence, the traditional concept and theory of bandwidth available for linear controllers cannot be directly applied to FCS-MPC. Nevertheless, a frequency-response analysis based on experiments and measurements could be performed as future developments.

VI. Applications of FCS-MPC

A. AFE Rectifiers

In regenerative applications, usually, active front-end (AFE) rectifiers, in back-to-back configuration with the inverter, are used. The critical part of the control scheme is to synchronize the system with the supply voltage and to control the dc-link voltage. This is generally implemented with voltage-oriented control or direct power control methods. In [35] and [36], the same application is controlled with FCS-MPC, controlling directly the active and reactive power of the system, without current control loops, as shown in Fig. 11. The cost function used for this application is

$$g = |Q_p| + |P^* - P_p| \quad (19)$$

where the reactive power reference is set to zero. Note that the inverter part of the back-to-back configuration is controlled separately with the FCS-MPC current control seen in Section III. The active power reference for the AFE (P^*) is computed by adding the power needed by the load (P^*_{load}) and the power necessary to control the dc-link capacitor P^*_{dc}. The prediction of the active power (P_p) is obtained by the measured supply voltage $\mathbf{v}_s(t_k)$ and current $\mathbf{i}_s(t_k)$ evaluated together with the switching states in the predictive model of the AFE and the supply interface RL branches.

The experimental behavior of the system for steps in the amplitude of the load current is shown in Fig. 12. This result has been obtained with a Dspace DS1103 control board with Matlab/Simulink installed on a host standard personal computer. The sample period used to implement this strategy is $T_s = 50\ \mu$s. Note how directly the active power reference reacts

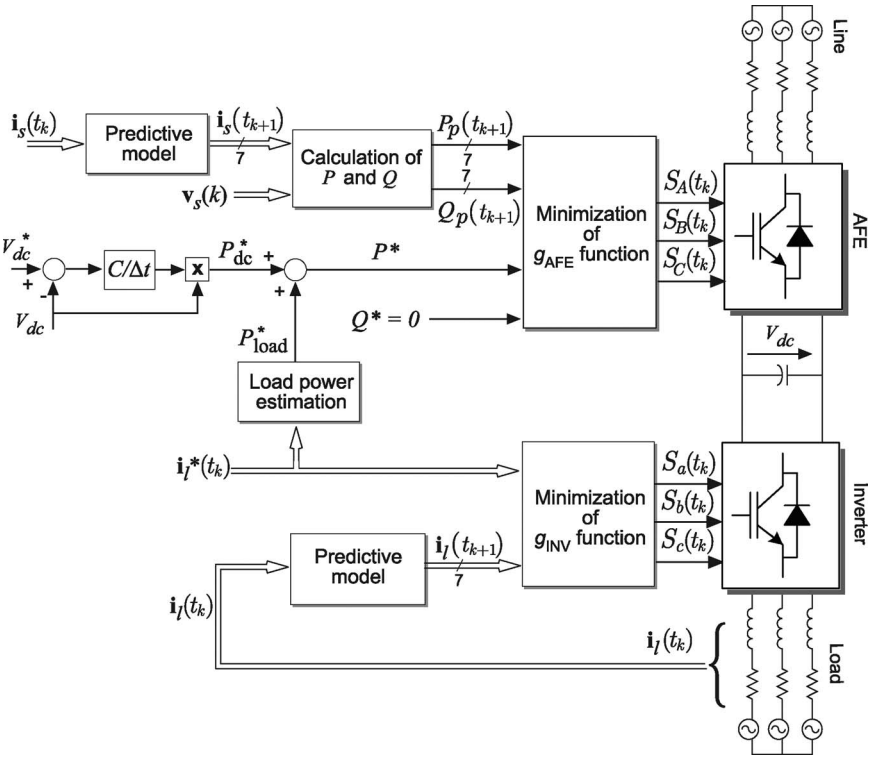

Fig. 11. Back-to-back FCS-MPC power control block diagram.

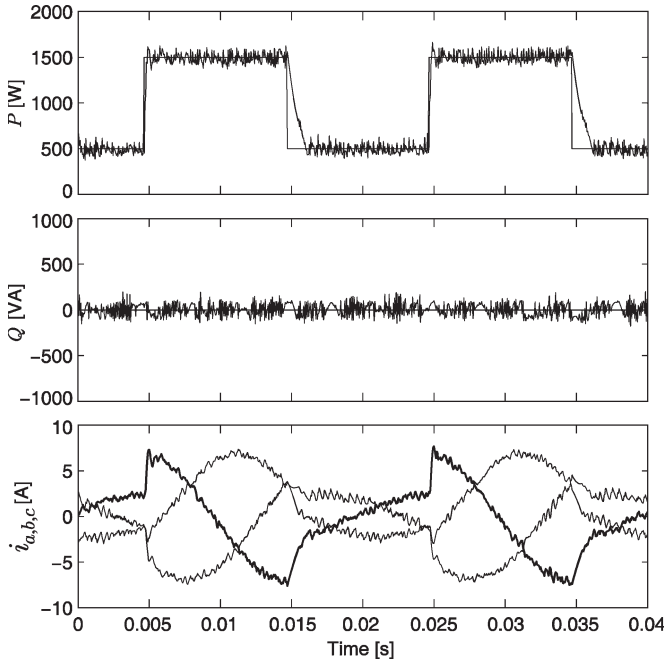

Fig. 12. Experimental FCS-MPC power control of a back-to-back converter with step change in load current. (a) Supply active power. (b) Supply reactive power. (c) Input currents.

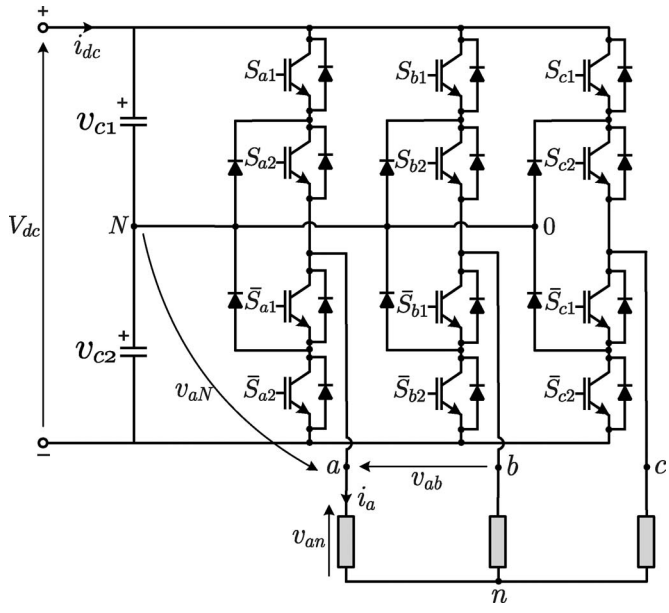

Fig. 13. NPC converter power circuit.

also as a step, which is properly followed by the FCS-MPC algorithm. The decoupling of the reactive power is successfully achieved even during the step transition. Note how the input current increases to supply the demanded active power. The input currents are sinusoidal, despite the fact that there are no current references or dedicated control loops. The input currents do not complete a full period due to the small time frame between steps in the active power.

B. NPC Multilevel Converter

The NPC converter is widely used in medium-voltage high-power applications. The power circuit is shown in Fig. 13. In this case, the objective is to control the load current, similar to the method presented for the 2L-VSI in Section III. However, there are two additional requirements: maintaining the voltage

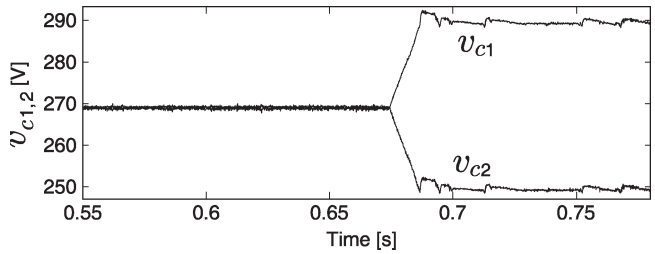

Fig. 14. Experimental FCS-MPC current control of NPC converter. Effect of the voltage balancing mechanism.

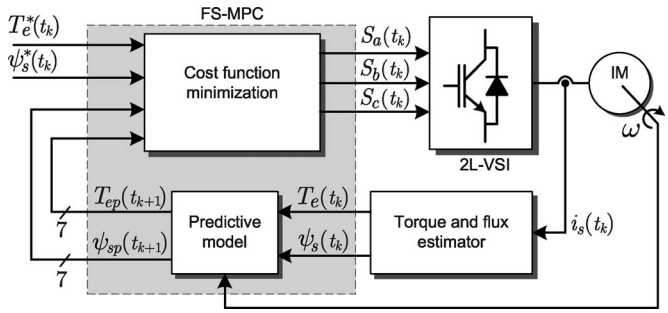

Fig. 15. FCS-MPC torque and flux control diagram.

balance of the dc-link capacitors and reducing power losses by avoiding unnecessary switchings in the power circuit. Those objectives are reflected in the following cost function:

$$g = |i_\alpha^* - i_{\alpha p}| + \left|i_\beta^* - i_{\beta p}\right| + \lambda_{\rm dc}|v_{c1p} - v_{c2p}| + \lambda_{\rm sw} C_p \quad (20)$$

where v_{c1p} and v_{c2p} are the predicted voltages of both dc-link capacitors and $\lambda_{\rm dc}$ and $\lambda_{\rm sw}$ are the weighting factors to adjust the dc-link balance and switching losses, respectively. A large value of certain λ's implies greater priority to achieve that objective. Fig. 7 shows the experimental output voltage and current of an NPC obtained with a traditional controller and with FCS-MPC. As mentioned before, the reduction in the switching losses was tested. In addition, Fig. 14 shows the behavior of the control method, with and without the dc-link control term in the cost function. Note that $\lambda_{\rm dc} = 0.1$ has been changed to zero at $t = 0.68$ s, losing the dc-link balancing control capability. As with results shown in Fig. 7, these experimental waveforms have been obtained with a Dspace DS1104 control board with Matlab/Simulink installed on a host standard personal computer. The sample period used to implement this strategy is $T_s = 100\ \mu$s.

C. Torque and Flux Control

Torque and flux control is mainly used for high-performance adjustable speed drives. In this application, the selection of the voltage vector is made by evaluating the effect of each one on the torque and flux of the machine model [52]–[54]. The torque reference T_e^* is obtained from the outer loop speed controller, while the reference stator flux magnitude $|\psi_s|^*$ is constant and defined by the rated machine values. The stator and rotor fluxes can be estimated with the measurement of the stator currents. Using the rotor speed and considering the seven possible voltage vectors, seven predictions of the torque and stator flux are calculated. A simplified control diagram is shown in Fig. 15. The control strategy is based on the minimization of a cost function g, given by

$$g = |T_e^* - T_e| + \lambda_\psi \left||\psi_s|^* - |\psi_s|\right| \quad (21)$$

where λ_ψ is a weighting factor that handles the magnitude relation between both terms.

Simulation results for a 2L-VSI-fed induction motor showing the drive startup, then a load torque step at $t = 0.3$ s, and the speed reversal at $t = 0.4$ s are shown in Fig. 16. This result has been obtained using Matlab/Simulink with a sample period $T_S = 50\ \mu$s. The torque presents a very good dynamic response

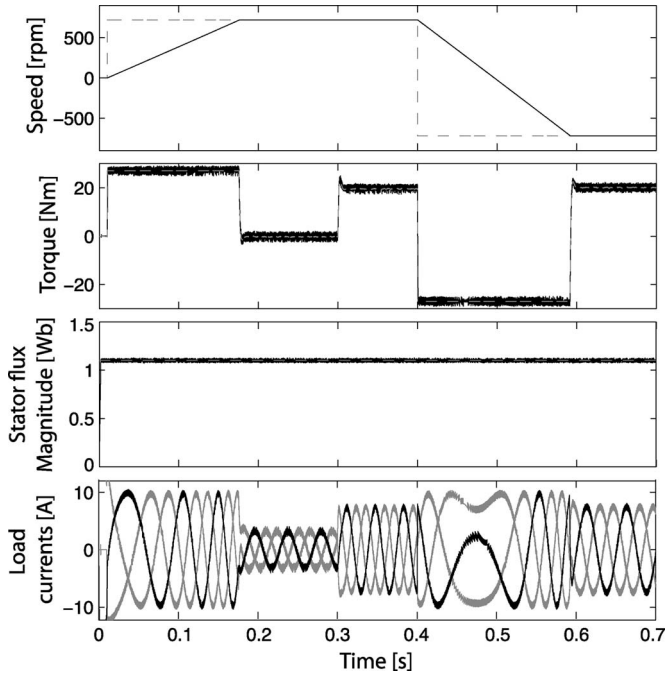

Fig. 16. FCS-MPC torque and flux control of an induction machine (simulation). Speed step response, torque dynamic behavior, stator flux, and load currents.

which is completely decoupled from the stator flux that is kept constant at all times, as can be clearly appreciated even during dynamic transitions. The load currents appear highly sinusoidal, although no current controllers are included in the control algorithm.

D. Matrix Converter

Matrix converters, such as the one shown in Fig. 17, are direct converter topologies which do not feature large energy storage components. These represent an alternative to the back-to-back converters, particularly in applications where size and volume are an issue [62]. The fact that matrix converters connect directly the mains to the load adds to the complexity of traditional controllers and modulation algorithms, since the input and output need to be controlled simultaneously. Here, FCS-MPC becomes very attractive, since the complete model can be used for prediction and several variables and requirements can be included in the cost function [52]–[54]. Fig. 18 shows the application of FCS-MPC to a matrix-converter-fed ac drive. Here, the cost function used is a combination of

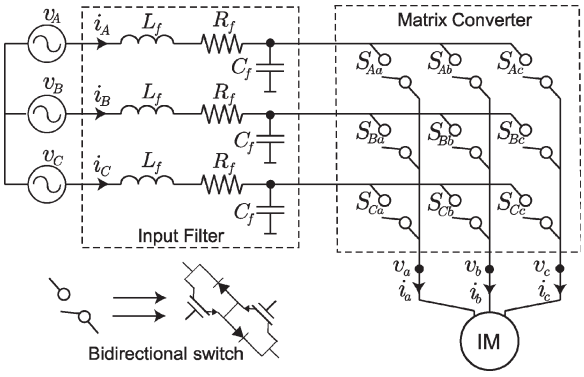

Fig. 17. Matrix converter power circuit.

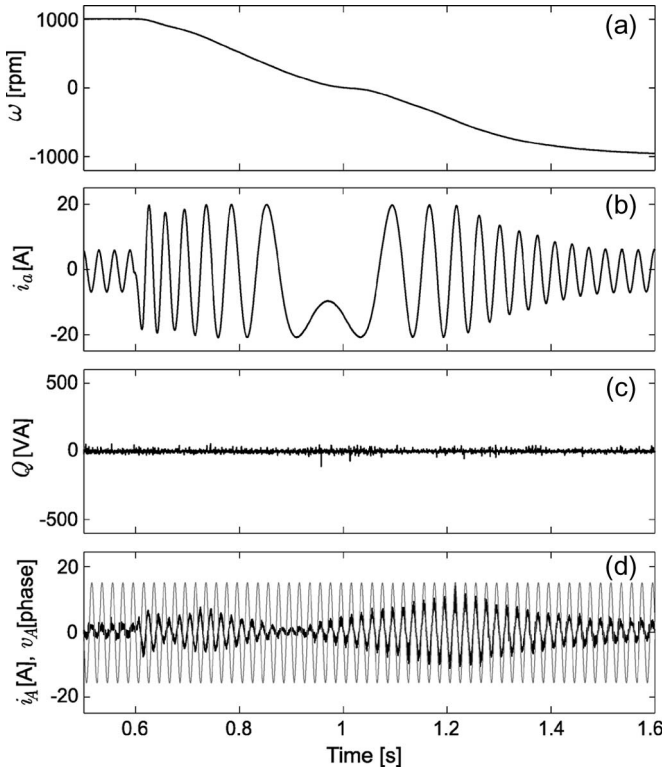

Fig. 18. Experimental FCS-MPC of a matrix-converter-fed ac drive during speed reversal. (a) Motor speed. (b) Load current. (c) Input reactive power. (d) Input voltage and current.

(21) for the torque and flux control, (16) to have zero reactive power (hence, synchronized sinusoidal input currents), and (13) to mitigate common-mode voltages at the converter output. Experimental results shown in Fig. 18 have been obtained with a Dspace DS1103 control board with Matlab/Simulink installed on a host standard personal computer. The sample period used to implement this strategy is $T_s = 8\ \mu$s. Again, the load current is completely sinusoidal, without current loops or modulators. The reactive power is properly controlled and remains zero at all times, resulting in sinusoidal input currents which are in phase with respect to the supply voltage. In Fig. 8, shown earlier, the effect of the common-mode voltage component can be appreciated.

Other interesting applications include active filters [60], flying capacitor controls [49], current source topologies [51], and UPSs [48].

VII. Conclusion

A general approach of FCS-MPC for power converters and drive applications has been presented. This control method is simple and allows for the control of different converters and various kinds of variables without the need of additional modulation techniques or internal cascade control loops. The drive signals for the power switches are generated directly by the controller. FCS-MPC is conceptually very simple yet powerful, since it considers, advantageously, the discrete nature of power converters and microprocessors. The required high calculation power that was a limitation some decades ago is overcome by today's standard DSPs and microcontrollers. Interesting applications can be found in those topologies where the modulation techniques are more complex, such as for matrix converters. However, the method can be applied without significant changes to any type of power converter or drive system.

One of the major advantages of FCS-MPC, and probably the greatest difference with traditional controllers, is the flexibility to control different variables, with constraints and additional system requirements (such as reactive power, common-mode voltages, switching losses, voltage unbalance, etc.). This can lead to improved performance, efficiency, and safety or to meet standards and operational limits demanded by the evolving industry applications. This is why FCS-MPC, with its great potential and flexibility, emerges as a promising tool for electric-power conversion.

References

[1] *Power Electronics Handbook*, 2nd ed. M. H. Rashid, Ed. New York: Academic, 2007.
[2] J. Holtz, "Pulsewidth modulation for power converters," *Proc. IEEE*, vol. 82, no. 8, pp. 1194–1214, Aug. 1994.
[3] J. Rodriguez, S. Bernet, B. Wu, J. Pontt, and S. Kouro, "Multilevel voltage-source-converter topologies for industrial medium-voltage drives," *IEEE Trans. Ind. Electron.*, vol. 54, no. 2, pp. 2930–2945, Dec. 2007.
[4] B. Wu, J. Pontt, J. Rodríguez, S. Bernet, and S. Kouro, "Current-source converter and cycloconverter topologies for industrial medium-voltage drives," *IEEE Trans. Ind. Electron.*, vol. 55, no. 7, pp. 2786–2797, Jul. 2008.
[5] C. K. Lau and M. H. Pong, "DSP based fuzzy controlled power converter operating in both continuous and discontinuous conduction modes," in *Proc. 22nd IEEE Int. Conf. Ind. Electron., Control, Instrum. (IECON)*, Aug. 5–10, 1996, vol. 3, pp. 1530–1535.
[6] W. Jun, P. Hong, and J. Yu, "A simple direct-torque fuzzy control of permanent magnet synchronous motor driver," in *Proc. 5th WCICA*, Jun. 15–19, 2004, vol. 5, pp. 4554–4557.
[7] P. J. Alsina and N. S. Gehlot, "Neuro-adaptive control of induction motor stator current," in *Proc. 21st IEEE Int. Conf. Ind. Electron., Control, Instrum. (IECON)*, Nov. 6–10, 1995, vol. 2, pp. 1434–1439.
[8] K. M. Tsang and W. L. Chan, "Adaptive control of power factor correction converter using nonlinear system identification," *Proc. Inst. Elect. Eng.—Elect. Power Appl.*, vol. 152, no. 3, pp. 627–633, May 6, 2005.
[9] S.-C. Tan, Y. M. Lai, and C. K. Tse, "Indirect sliding mode control of power converters via double integral sliding surface," *IEEE Trans. Power Electron.*, vol. 23, no. 2, pp. 600–611, Mar. 2008.
[10] F. Cupertino, A. Lattanzi, and L. Salvatore, "Sliding mode control of an induction motor," in *Proc. 8th Int. Conf. Power Electron. Variable Speed Drives*, 2000, pp. 206–211.
[11] R. Kennel and A. Linder, "Predictive control of inverter supplied electrical drives," in *Proc. IEEE PESC*, Galway, Ireland, 2000, pp. 761–766.
[12] O. Kukrer, "Discrete-time current control of voltage-fed three-phase PWM inverters," *IEEE Trans. Ind. Electron.*, vol. 11, no. 2, pp. 260–269, Mar. 1996.

[13] H. Le-Huy, K. Slimani, and P. Viarouge, "Analysis and implementation of a real-time predictive current controller for permanent-magnet synchronous servo drives," *IEEE Trans. Ind. Electron.*, vol. 41, no. 1, pp. 110–117, Feb. 1994.

[14] H.-T. Moon, H.-S. Kim, and M.-J. Youn, "A discrete-time predictive current control for PMSM," *IEEE Trans. Power Electron.*, vol. 18, no. 1, pp. 464–472, Jan. 2003.

[15] L. Springob and J. Holtz, "High-bandwidth current control for torque-ripple compensation in PM synchronous machines," *IEEE Trans. Ind. Electron.*, vol. 45, no. 5, pp. 713–721, Oct. 1998.

[16] S. J. Henriksen, R. E. Betz, and B. J. Cook, "Practical issues with predictive current controllers," in *Proc. Australas. Univ. Power Eng. Conf.*, 2001, pp. 526–530.

[17] G. Bode, P. C. Loh, M. J. Newman, and D. G. Holmes, "An improved robust predictive current regulation algorithm," *IEEE Trans. Ind. Appl.*, vol. 41, no. 6, pp. 1720–1733, Nov./Dec. 2005.

[18] S.-M. Yang and C.-H. Lee, "A deadbeat current controller for field oriented induction motor drives," *IEEE Trans. Power Electron.*, vol. 17, no. 5, pp. 772–778, Sep. 2002.

[19] H. Abu-Rub, J. Guzinski, Z. Krzeminski, and H. A. Toliyat, "Predictive current control of voltage source inverters," *IEEE Trans. Ind. Electron.*, vol. 51, no. 3, pp. 585–593, Jun. 2004.

[20] L. Malesani, P. Mattavelli, and S. Buso, "Robust dead-beat current control for PWM rectifier and active filters," *IEEE Trans. Ind. Appl.*, vol. 35, no. 3, pp. 613–620, May/Jun. 1999.

[21] W. Zhang, G. Feng, and Y.-F. Liu, "Analysis and implementation of a new PFC digital control method," in *Proc. IEEE PESC*, Acapulco, Mexico, 2003, pp. 335–340.

[22] S.-G. Jeong and M.-H. Woo, "DSP-based active power filter with predictive current control," *IEEE Trans. Ind. Electron.*, vol. 44, no. 3, pp. 329–336, Jun. 1997.

[23] J. Mossoba and P. W. Lehn, "A controller architecture for high bandwidth active power filters," *IEEE Trans. Power Electron.*, vol. 18, no. 1 pt. 2, pp. 317–325, Jan. 2003.

[24] S. Buso, S. Fasolo, and P. Mattavelli, "Uninterruptible power supply multiloop employing digital predictive voltage and current regulators," *IEEE Trans. Ind. Appl.*, vol. 37, no. 6, pp. 1846–1854, Nov./Dec. 2001.

[25] P. Mattavelli, "An improved deadbeat control for UPS using disturbance observers," *IEEE Trans. Ind. Electron.*, vol. 52, no. 1, pp. 206–212, Feb. 2005.

[26] E. F. Camacho and C. Bordons, *Model Predictive Control*. New York: Springer-Verlag, 1999.

[27] A. Linder and R. Kennel, "Model predictive control for electrical drives," in *Proc. IEEE PESC*, Recife, Brazil, Jun. 12–16, 2005, pp. 1793–1799.

[28] R. Kennel, A. Linder,and M. Linke, "Generalized predictive control (GPC)-ready for use in drive applications?" in *Proc. 32nd Annu. IEEE PESC*, 2001, vol. 4, pp. 1839–1844.

[29] S. Muller, U. Ammann, and S. Rees, "New modulation strategy for a matrix converter with a very small mains filter," in *Proc. 33rd IEEE PESC*, Acapulco, Mexico, 2003, pp. 1275–1280.

[30] J. Rodríguez, J. Pontt, C. Silva, M. Salgado, S. Rees, U. Ammann, P. Lezana, R. Huerta, and P. Cortés, "Predictive control of a three-phase inverter," *Electron. Lett.*, vol. 40, no. 9, pp. 561–562, Apr. 29, 2004.

[31] J. Rodriguez, J. Pontt, C. Silva, P. Cortes, U. Amman, and S. Rees, "Predictive current control of a voltage source inverter," in *Proc. 35th IEEE PESC*, Jun. 2004, vol. 3, pp. 2192–2196.

[32] J. Rodríguez, J. Pontt, C. Silva, P. Correa, P. Lezana, P. Cortés, and U. Ammann, "Predictive current control of a voltage source inverter," *IEEE Trans. Ind. Electron.*, vol. 54, no. 1, pp. 495–503, Feb. 2007.

[33] J. Rodriguez, J. Pontt, P. Cortes, and R. Vargas, "Predictive control of a three-phase neutral point clamped inverter," in *Proc. IEEE 36th PESC*, 2005, pp. 1364–1369.

[34] S. Muller, U. Ammann, and S. Rees, "New time-discrete modulation scheme for matrix converters," *IEEE Trans. Ind. Electron.*, vol. 52, no. 6, pp. 1607–1615, Dec. 2005.

[35] J. Rodriguez, J. Pontt, P. Correa, U. Ammann, and P. Cortes, "Novel control strategy of an AC/DC/AC converter using power relations," in *Proc. Int. Conf. PELINCEC*, Warsaw, Poland, Oct. 16–19, 2005.

[36] J. Rodriguez, J. Pontt, P. Correa, P. Lezana, and P. Cortes, "Predictive power control of an AC/DC/AC converter," in *Conf. Rec. IEEE IAS Annu. Meeting*, Oct. 2005, vol. 2, pp. 934–939.

[37] J. Rodriguez, J. Pontt, C. Silva, P. Cortés, S. Rees, and U. Ammann, "Predictive direct torque control of an induction machine," in *Proc. 11th Int. EPE-PEMC*, Riga, Latvia, Sep. 2–4, 2004.

[38] P. Cortes, J. Rodriguez, D. E. Quevedo, and C. Silva, "Predictive current control strategy with imposed load current spectrum," *IEEE Trans. Power Electron.*, vol. 23, no. 2, pp. 612–618, Mar. 2008.

[39] P. Cortes, J. Rodriguez, R. Vargas, and U. Ammann, "Cost function-based predictive control for power converters," in *Proc. 32nd Annu. IEEE IECON*, Nov. 2006, pp. 2268–2273.

[40] D. E. Quevedo and G. C. Goodwin, "Control of EMI from switch-mode power supplies via multi-step optimization," in *Proc. Amer. Control Conf.*, Jun./Jul. 2004, vol. 1, pp. 390–395.

[41] M. Catucci, J. Clare, and P. Wheeler, "Predictive control strategies for ZCS direct converter HV power supply," in *Proc. Eur. Conf. Power Electron. Appl.*, Sep. 2005.

[42] A. Linder and R. Kennel, "Direct model predictive control—A new direct predictive control strategy for electrical drives," in *Proc. Eur. Conf. Power Electron. Appl.*, Sep. 2005.

[43] D. E. Quevedo and G. C. Goodwin, "Multistep optimal analog-to-digital conversion," *IEEE Trans. Circuits Syst. I, Reg. Papers*, vol. 52, no. 3, pp. 503–515, Mar. 2005.

[44] G. Perantzakis, F. Xepapas, S. Papathanassiou, and S. N. Manias, "A predictive current control technique for three-level NPC voltage source inverters," in *Proc. 36th IEEE PESC*, Sep. 2005, pp. 1241–1246.

[45] G. S. Perantzakis, F. H. Xepapas, and S. N. Manias, "Efficient predictive current control technique for multilevel voltage source inverters," in *Proc. Eur. Conf. Power Electron. Appl.*, Sep. 2005.

[46] H. Q. S. Dang, P. Wheeler, and J. Clare, "A control analysis and implementation of high voltage, high frequency direct power converter," in *Proc. 32nd Annu. IEEE IECON*, Nov. 2006, pp. 2096–2102.

[47] M. Catucci, J. Clare, and P. Wheeler, "Predictive control strategy for ZCS single stage resonant converter," in *Proc. 32nd Annu. IEEE IECON*, Nov. 2006, pp. 2905–2910.

[48] P. Cortes and J. Rodriguez, "Three-phase inverter with output LC filter using predictive control for UPS applications," in *Proc. Eur. Conf. Power Electron. Appl.*, Sep. 2007, pp. 1–7.

[49] E. I. Silva, B. P. McGrath, D. E. Quevedo, and G. C. Goodwin, "Predictive control of a flying capacitor converter," in *Proc. Amer. Control Conf.*, New York, Jul. 2007, pp. 3763–3768.

[50] R. Vargas, P. Cortes, U. Ammann, J. Rodriguez, and J. Pontt, "Predictive control of a three-phase neutral-point-clamped inverter," *IEEE Trans. Ind. Electron.*, vol. 54, no. 5, pp. 2697–2705, Oct. 2007.

[51] P. Correa, J. Rodriguez, and P. Cortes, "A predictive control scheme for current source rectifiers," in *Proc. 13th EPE-PEMC*, Poznan, Poland, Sep. 1–3, 2008, pp. 699–702.

[52] J. Rodríguez, J. Pontt, R. Vargas, P. Lezana, U. Ammann, P. Wheeler, and F. García, "Predictive direct torque control of an induction motor fed by a matrix converter," in *Proc. EPE Conf.*, Aalborg, Denmark, 2007, pp. 1–10.

[53] M. Rivera, J. Espinoza, R. Vargas, and J. Rodríguez, "Behavior of the predictive DTC based matrix converter under unbalanced AC supply," in *Conf. Rec. IEEE IAS Annu. Meeting*, New Orleans, LA, Sep. 23–27, 2007, pp. 202–207.

[54] R. Vargas, M. Rivera, J. Rodríguez, and J. Espinoza, "Predictive torque control with input PF correction applied to an induction machine fed by a matrix converter," in *Proc. IEEE PESC*, Jun. 15–19, 2008, pp. 9–14.

[55] R. Vargas, U. Ammann, J. Rodríguez, and J. Pontt, "Predictive strategy to reduce common-mode voltages on power converters," in *Proc. IEEE PESC*, Jun. 15–19, 2008, pp. 3401–3406.

[56] R. Vargas, U. Ammann, J. Rodríguez, and J. Pontt, "Reduction of switching losses and increase in efficiency of power converters using predictive control," in *Proc. IEEE PESC*, Jun. 15–19, 2008, pp. 1062–1068.

[57] G. Goodwin, S. Graebe, and M. Salgado, *Control System Design*. Englewood Cliffs, NJ: Prentice-Hall, 2001.

[58] L. Asiminoaei, P. Rodríguez, and F. Blaabjerg, "Application of discontinuous PWM modulation in active power filters," *IEEE Trans. Power Electron.*, vol. 23, no. 4, pp. 1692–1706, Jul. 2008.

[59] U. Ammann, R. Vargas, S. Rees, J. Serra, and J. Roth-Stielow, "An analytical approach to steady-state current control properties of power converters featuring discrete-time switching," in *Proc. IEEE PESC*, Jun. 15–19, 2008, pp. 2535–2542.

[60] D. Nedeljkoviè, M. Nemec, and V. Ambrožiè, "Three-phase parallel active power filter with direct current control," in *Proc. EPE-PEMC*, Portoro, Slovenia, 2006, pp. 1660–1664.

[61] V. Ambrožiè, R. Fišer, and D. Nedeljkoviè, "Direct current control—A new current regulation principle," *IEEE Trans. Power Electron.*, vol. 18, no. 1, pp. 495–503, Jan. 2003.

[62] P. Wheeler, J. Rodriguez, J. Clare, L. Empringham, and A. Weinstein, "Matrix converters: A technology review," *IEEE Tran. Ind. Electron.*, vol. 49, no. 2, pp. 276–288, Apr. 2002.

[63] P. Cortes, S. Kouro, B. La Rocca, R. Vargas, J. Rodriguez, J. I. Leon, S. Vazquez, and L. G. Franquelo, "Guidelines for weighting factors design in model predictive control of power converters and drives," in *Proc. IEEE ICIT*, Gippsland, Australia, Feb. 10–13, 2009.

Samir Kouro (S'04–M'08) was born in Valdivia, Chile, in 1978. He received the M.Sc. and Ph.D. degrees in electronics engineering from the Universidad Técnica Federico Santa María (UTFSM), Valparaíso, Chile, in 2004 and 2008, respectively.

He joined the Electronics Engineering Department, UTFSM, as a Research Assistant in 2004 and became an Associate Researcher in 2008. Since 2009, he has been a Postdoctoral Fellow at Ryerson University, Toronto, ON, Canada. His main research interests include power converters, adjustable-speed drives, and renewable energy power systems.

Dr. Kouro was distinguished by the President of the Republic as the youngest researcher of the Chilean National Fund of Scientific and Technological Development (FONDECYT) in 2004. He was also the recipient of the "Ismael Valdés Award" from the Institute of Engineers of Chile in 2005, in recognition of his ability to organize and direct moral conditions and technical preparation.

Patricio Cortés (S'05–M'08) received the Engineer and M.Sc. degrees in electronics engineering and the Ph.D. degree from the Universidad Técnica Federico Santa María (UTFSM), Valparaíso, Chile, in 2004 and 2008 respectively.

Since 2003, he has been with the Electronics Engineering Department, UTFSM where he is currently a Research Associate. In 2007, he was a Visiting Scholar with the Institute of Control and Industrial Electronics, Warsaw University of Technology, Warsaw, Poland. His main research interests are power electronics, adjustable-speed drives, and predictive control. He received the IEEE TRANSACTIONS ON INDUSTRIAL ELECTRONICS Best Paper Award in 2007 from the IEEE Industrial Electronics Society.

René Vargas (S'05) received the Engineer and M.Sc. (with honors) degrees in electronics engineering from the Universidad Técnica Federico Santa María (UTFSM), Valparaíso, Chile, in 2005, where he is currently working toward the Ph.D. degree in the Electronics Engineering Department.

He was with the Institute of Power Electronics and Electrical Drives, Universität Stuttgart, Stuttgart, Germany, during scientific stays in 2006, 2007, and 2008. His main research interests include predictive control, matrix converters, and new control techniques applied to power conversion and drives.

Ulrich Ammann (M'06) received the Dipl.-Ing. degree in electrical engineering from the Universität Stuttgart, Stuttgart, Germany, in 2002, where he is currently working toward the Ph.D. degree in the field of discrete-time modulation schemes, including predictive techniques.

Since 2002, he has been with the Institute of Power Electronics and Control Engineering, Universität Stuttgart, as a Research Assistant. His research interests include electric drives, high-power current sources, and automotive power electronics.

José Rodríguez (M'81–SM'99) received the Engineer degree in electrical engineering from the Universidad Técnica Federico Santa María (UTFSM), Valparaíso, Chile, in 1977, and the Dr.-Ing. degree in electrical engineering from the University of Erlangen, Erlangen, Germany, in 1985.

Since 1977, he has been a Professor with the UTFSM, where, from 2001 to 2004, he was the Director of the Electronics Engineering Department, from 2004 to 2005, he was the Vice Rector of academic affairs, and, since 2005, he has been Rector. During his sabbatical leave in 1996, he was with Siemens Corporation, Santiago, Chile, where he was responsible for the mining division. He has extensive consulting experience in the mining industry, particularly in the application of large drives, such as cycloconverter-fed synchronous motors for SAG mills, high-power conveyors, controlled ac drives for shovels, and power-quality issues. He has directed over 40 R&D projects in the field of industrial electronics; he has coauthored over 250 journal and conference papers and has contributed one book chapter. His research group has been recognized as one of the two centers of excellence in engineering in Chile in the years 2005 and 2006. His main research interests include multilevel inverters, new converter topologies, and adjustable-speed drives.

Prof. Rodríguez is an active Associate Editor of the IEEE Power Electronics and IEEE Industrial Electronics Societies since 2002. He has served as the Guest Editor of the IEEE TRANSACTIONS ON INDUSTRIAL ELECTRONICS in five opportunities [Special Sections on Matrix Converters (2002), Multilevel Inverters (2002), Modern Rectifiers (2005), High-Power Drives (2007), and Predictive Control of Power Electronic Drives (2008)].